SCANNING VOL. 27, 240–248 (2005)

Received: February 3, 2005
Accepted with revision: June 6, 2005

Mineral Content Changes in Bone Associated with Damage Induced by the Electron Beam

ROY D. BLOEBAUM, PH.D., JENNIFER L. HOLMES, M.D., M.S., JOHN G. SKEDROS, M.D.

Bone and Joint Research Laboratory, Department of Veterans Affairs (VA) Medical Center, Salt Lake City, Utah, USA

Summary: Energy-dispersive x-ray (EDX) spectroscopy and backscattered electron (BSE) imaging are finding increased use for determining mineral content in microscopic regions of bone. Electron beam bombardment, however, can damage the tissue, leading to erroneous interpretations of mineral content. We performed elemental (EDX) and mineral content (BSE) analyses on bone tissue in order to quantify observable deleterious effects in the context of (1) prolonged scanning time, (2) scan versus point (spot) mode, (3) low versus high magnification, and (4) embedding in poly-methylmethacrylate (PMMA). Undemineralized cortical bone specimens from adult human femora were examined in three groups: 200× embedded, 200× unembedded, and 1000× embedded. Coupled BSE/EDX analyses were conducted five consecutive times, with no location analyzed more than five times. Variation in the relative proportions of calcium (Ca), phosphorous (P), and carbon (C) were measured using EDX spectroscopy, and mineral content variations were inferred from changes in mean gray levels ("atomic number contrast") in BSE images captured at 20 keV. In point mode at 200×, the embedded specimens exhibited a significant increase in Ca by the second measurement (7.2%, $p < 0.05$); in scan mode, a small and statistically nonsignificant increase (1.0%) was seen by the second measurement. Changes in P were similar, although the increases were less. The apparent increases in Ca and P likely result from decreases in C: –3.2% ($p < 0.05$) in point mode and –0.3% in scan mode by the second measurement. Analysis of unembedded specimens showed similar results. In contrast to embedded specimens at 200×, 1000× data showed significantly larger variations in the proportions of Ca, P, and C by the second or third measurement in scan and point mode. At both magnifications, BSE image gray level values increased (suggesting increased mineral content) by the second measurement, with increases up to 23% in point mode. These results show that mineral content measurements can be reliable when using coupled BSE/EDX analyses in PMMA-embedded bone if lower magnifications are used in scan mode and if prolonged exposure to the electron beam is avoided. When point mode is used to analyze minute regions, adjustments in accelerating voltages and probe current may be required to minimize damage.

Key words: energy-dispersive x-ray spectroscopy, bone, backscattered electron imaging, bone mineralization, osteon

PACS: 07.78. + S, 41.75.Fr

Introduction

Atomic-number-contrast backscattered electron (BSE) imaging and energy-dispersive x-ray (EDX) spectroscopy are finding increased use for quantifying mineral content variations in microscopic regions of bone (Boyde *et al*. 1998, Loveridge *et al*. 2004, Misof *et al*. 2003, Roschger *et al*. 1997, 1998; Skedros *et al*. 2005). However, ensuring accuracy has been challenging since electron bombardment can damage the analyzed region, resulting in erroneous interpretations of mineral content. Few studies have quantitatively examined this issue. In this perspective, the general goals of the present study are two-fold (specific hypotheses tested are listed below): (1) quantify damage-induced changes in mineral content of bone during BSE and EDX analyses, and (2) determine whether damage-induced changes in proportions of light elements such as carbon (C), in comparison with the heavier elements calcium (Ca) and phosphorus (P), can explain these artifactual changes in mineral content.

Electron beam-induced damage can be significant even when conventional operating conditions are used in BSE analyses of bone (Boyde and Jones 1996, Vajda *et al*. 1998). This damage includes the disruption of chemical bonds, the production and dispersal of molecular fragments,

This research was funded by the Bone and Joint Research Laboratory and the Department of Veterans Affairs (VA) Medical Research Fund from the Salt Lake City VA Healthcare System.

Address for reprints:

Roy D. Bloebaum, Ph.D.
Co-Director Bone and Joint Research Laboratory (151F)
Department of Veterans Affairs (VA)
Salt Lake City Health Care System
500 S. Foothill Blvd.
Salt Lake City, UT 84148-9998, USA
e-mail: Roy.Bloebaum@hsc.utah.edu

and mass loss (Acosta *et al.* 1993, Fryer and McConnell 1992, Isaacson 1977, Thach and Thach 1971, von Zglinicki 1993). In BSE images of bone, Boyce *et al.* (1990) described this observable damage as "bleaching" since image gray levels became notably brighter (Fig. 1). This "bleaching" has been attributed to "burning off" of low-atomic-number elements (e.g., carbon and oxygen) (Everhart *et al.* 1972, Goldstein *et al.* 1992), which can lead to erroneous interpretations of mineral content since gray levels in BSE images of bone correlate strongly with mineral content (Bloebaum *et al.* 1997, Skedros *et al.* 1993a,b).

Reduction in C and oxygen (O), and the consequent increase in relative proportions of Ca and P, can also change electron interaction and x-ray generation volumes (e.g., they can become larger), possibly further increasing the potential for error in microanalysis of bone mineralization by the inadvertent inclusion of tissue beyond the visualized microscopic field (Boyde and Jones 1996, Goldstein *et al.* 1992, Nicholson and Dempster 1980, Skedros *et al.* 2005, Weavers 1975). This is important for quantifying mineralization or composition differences between minute regions of bone microstructure, for example when comparing mineral content in cement lines with adjacent bone. Point (spot) mode might be required in these situations or in analyses of nearby regions that are susceptible to confounding influences of overlap of x-ray/electron interaction volumes (Skedros *et al.* 2005). However, compared with scan mode, point mode could produce increased damage because of relatively greater energy absorbed when using the smaller analyzed volume and longer dwell time of the electron beam. We have observed similar differences in bone tissue damage between low magnification (e.g., 200×) and high magnification (e.g., 1000×), which might similarly be related to greater energy absorbed by the analyzed region at higher magnification (Holmes *et al.* 2000).

In this study we performed elemental (EDX) and mineral content (BSE) analyses on bone tissue in order to quantify consequences of the observable deleterious effects of the electron beam in the context of (1) prolonged scanning time, (2) scan versus point mode, (3) low versus high magnification, and (4) embedding in poly-methylmethacrylate (PMMA). Undemineralized cortical bone specimens from adult human femora were examined in three groups: 200× embedded, 200× unembedded, and 1000× embedded. Coupled BSE/EDX analyses were conducted at each of five consecutive times, which allowed for the quantification of temporal changes in the proportions of low versus high atomic number elements and changes in apparent mineral content. The following hypotheses were tested:

1. Prolonged scan time will reveal that some scanning conditions produce obvious damage by the second measurement
2. Point mode is more deleterious than scan mode
3. High magnification (1000×) is more deleterious than low magnification (200×)
4. The electron beam damage in PMMA-embedded bone will be significantly less than in unembedded bone
5. Apparent increases in mineral content with successive analyses in the same image field can be attributed to changes in relative proportions of C, Ca, and P, primarily because C "burns off" early in analysis.

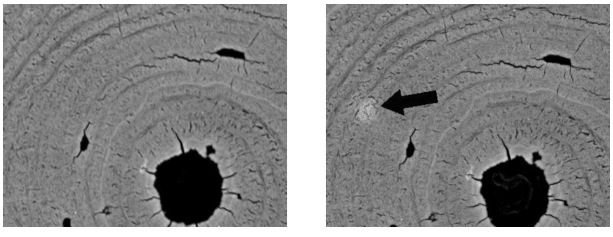

(a) (b)

FIG. 1 The arrow indicates a region of increased brightness, suggesting increased mean atomic number, at the location where the beam was positioned for five serial analyses in point mode at 1000×. The analyzed region is located within the wall of a double-zoned secondary osteon (i.e., a small osteon within a larger osteon). This increase is attributable to beam damage that causes the collagen (Z ~ 6) and PMMA (Z ~ 6.5) to be vaporized, leaving the mineral behind. The resulting "bleached" analysis region is ~11 × 11 microns. The osteonal central canal is at the lower right of the image.

Materials and Methods

Specimen Collection and Preparation

Fourteen human femora were obtained from skeletally mature males and females (age range 19–87 years). Medical records revealed no history of medications (e.g., glucocorticoids and bisphosphonates), diseases, pathologies, or abnormal blood chemistries that might have affected metabolism or mechanical competence of the donor bone. After being manually dissected free of soft tissue, each bone was measured on an osteometric table (Kuo *et al.* 1998, Ruff and Hayes 1983). Transverse cuts were then made at mid-diaphysis, producing one 5 mm-thick segment from each bone.

Two specimens, each measuring ~10 mm in medial-lateral width, were cut from the anterior cortex of each segment and stored in 70% ethyl alcohol (EtOH) for several months. One half of the specimens was processed for embedding and the others were not embedded. Embedding included dehydration in ascending concentrations of EtOH, clearing in xylene, and embedding in poly-methylmethacrylate (PMMA) (Sanderson and Kitabayashi 1994). The embedded specimens were glued together with cyanoacrylate glue to form two specimen aggregates.

Unembedded bone specimens were dried for several months over anhydrous $CaSO_4$ (Drierite, W.A. Hammond Drierite Co., Xenia, Ohio, USA). These specimens were then placed into holes that were drilled into a Plexiglas™ block and were anchored peripherally with fast-drying epoxy; this ensured that the glue did not penetrate into the central por-

tion of the specimens where the microscopic analyses would be conducted. A pure magnesium wire (Johnson Matthey, Inc., Seabrook, N.H., USA) was placed into a drill hole that was made in each specimen aggregate. As described below, this was used to ensure that no significant fluctuations in the electron beam stability occurred during the experiments.

The blocks containing the embedded and unembedded bone specimens were ground and polished with a buffing (revolving) wheel to achieve an optically smooth, scratch-free surface (Bloebaum *et al*. 1990) that was co-planar with the anatomical transverse plane in which the bone segments were originally cut; the buffing wheel is commonly used in lapidary work. Polishing was done under a continuous water stream and using α-alumina (1.0 micron, Fusco Abrasives, Tempe, Ariz., USA). This method is typically used for preparing PMMA-embedded specimens for BSE imaging and reduces surface topography to a sufficient level for purposes of the present study (Vajda *et al*. 1999). Each block was then lightly sputtercoated with gold for 60 s at 70 mTorr and 10 mA (Hummer VI-A, Anatech Ltd., Alexandria, Va., USA), resulting in a gold layer of approximately 250 Å that prevented charging of the specimen during imaging.

Energy-Dispersive X-ray and Backscattered Electron Analysis

Experiments in this study were performed with a JEOL 6100 SEM (JEOL, USA, Inc., Peabody, Mass., USA) configured with an EDX detector and interfaced with a computer (see below). Three unembedded and four PMMA-embedded specimens were used for analysis in scan mode, which was conducted in five randomly selected regions of each specimen. Three additional unembedded and four additional PMMA-embedded specimens were used for point (spot) mode data, with analysis in five randomly selected regions of each specimen. At each measurement "time," one BSE image was captured (requiring ~30 s), and then one x-ray spectrum was obtained and analyzed (requiring ~64 s: 60-s x-ray collection time and 4-s data processing time). These settings allowed for the collection of ~250,000 photon counts per EDX spectrum. The five coupled BSE/EDX analyses were conducted in sequence, and no location was analyzed more than five times. Additional measures taken to minimize beam induced damage included (1) placing the beam on standby (diverting energy from the specimen) between image locations and between analyses within the same image location, and (2) determining mineral content, represented by BSE image mean gray level, of each digitized image after completion of the entire imaging session. To ensure beam stability, gray level analysis (see below) was conducted on BSE images of the Mg standard at the beginning and end of each imaging session (Skedros *et al*. 1993a).

Energy-dispersive x-ray spectroscopy was performed using a lithium-drifted silicon EDX detector (Pentafet, Oxford Instruments, Cambridge, UK) equipped with a beryllium window. The operating conditions used for EDX analysis included 20 keV accelerating voltage, 2.5 nA probe current, and 15 mm working distance. The EDX data were compiled for analysis using the Link ISIS system (Oxford Instruments). Calibration standards included 99.99% pure calcium carbonate ($CaCO_3$) and indium phosphide (InP) (Tousimis Research Inc., Rockville, Md., USA). Relative percentages of Ca and P were measured using commercially available ZAF-correction software (SEMQuant, Oxford Instruments). The remaining lighter elements [hydrogen (H), C, nitrogen (N), and O] were characterized as "nonanalyzed elements", with C selected as the dominant matrix element in accordance with ZAF-correction methods described by Roschger *et al*. (1995). This method does not measure stoichiometric changes in the mineral phase, but rather overall changes in the apparent concentration of all of the measured elements. To ensure uniform operating conditions, gain calibrations were made using the K-α line of copper after every set of five BSE/EDX measurements (Vajda *et al*. 1996).

For EDX analyses, 35 random regions were analyzed in the scan mode and 35 random regions were analyzed in point mode. Scan and point mode data were obtained from independent locations. At 200×, the analyzed area in scan mode was 460.0 × 460.0 microns and in point mode 54.5 × 54.5 microns. At 1000×, the analyzed area in scan mode was 92.0 × 92.0 microns and in point mode 10.9 × 10.9 microns. Due to limitations in our equipment, the energy absorbed by the specimen could not be directly measured. Consequently, rigorous comparisons in this context between scan and point mode could not be made. Nevertheless, in these two modes the ultimate consequences of electron beam bombardment were quantified; namely, changes in proportions of Ca, P, and C, and observable changes in apparent mineralization in BSE images.

In scan mode, an initial BSE image was digitally captured at 200× magnification (Link ISIS System, Oxford Instruments, Oxford, UK) using nine scans and a Kalman frame averaging technique (Oxford Instruments). In image selection, care was taken to avoid porous spaces represented by primary and secondary vascular canals and Volkmann's canals. However, porosities represented by lacunae and canaliculi could not be entirely avoided. Consequently, these porosities, although minute, can influence the EDX spectra, but not the BSE image gray level (mineral content) data since their influence can be eliminated (see below). The EDX spectrum was subsequently collected (described above) from the region represented by the entire BSE image. Once the spectrum was complete, the probe current was checked and manually adjusted as needed; this ensured consistent image contrast (Holmes *et al*. 2000, Vajda *et al*. 1996). Four additional coupled BSE/EDX measurements were conducted at the same location. This allowed for correlation of apparent mineral content changes during capture of the five successive BSE images that were coupled with the five successive EDX spectra.

For point mode data, the BSE images at 200X magnification were collected as described above for scan mode,

but the beam was focused within a lamella of a secondary osteon. Five consecutive EDX spectra were collected at this location, with the probe current monitored and adjusted as needed between spectra. To reduce specimen damage in point mode, mean gray level (mineral content) data were collected only at the first and fifth measurement.

Using additional specimens of embedded bone tissue, measurements were also made at 1000× in scan and point modes. Unembedded specimens were not used in this analysis since the charging of the unembedded specimens rendered it impossible to obtain good images as well as reliable data. The protocol for the measurements and analysis in the embedded 1000× images was the same as described above, with five consecutive coupled BSE/EDX analyses in scan mode and two in point mode. Only two analyses were done in point mode because the subsequent damage was so extensive that significant specimen surface charging occurred, rendering further analyses difficult. Numerical gray level values (0, 1, 2, 3 ... 255) in the digitized BSE images were determined for each pixel using a public domain software package from the public domain National Institutes of Health (NIH) Image (1.55) software (http://rsb.info.nih.gov/ nih-image/). A "weighted mean gray level" value, which correlates with the degree of mineral content, and hence density (g/cm^3) (Skedros *et al*. 1993a,b), was calculated for each BSE image. To eliminate the influence of porous spaces (e.g., canaliculi, lacunae, and vascular spaces), gray levels 0–5 were removed from the calculation. This procedure serves to reduce the influence of the spread of the PMMA peak from the gray level histogram (Bloebaum *et al*. 1997).

Changes between consecutive analyses were evaluated for statistical significance using a one-way analysis of variance (ANOVA) design and Fisher's PLSD post-hoc test (StatView version 5.0, SAS Institute Inc., Cary, N.C., USA). A p value of ≤ 0.05 was considered statistically significant.

Results

Element Energy-Dispersive X-ray Analysis

At 200X, EDX data in point mode from both embedded and unembedded specimens showed significant changes in the relative proportions of Ca, P, and C by the second measurement (exception: in embedded specimens, P did not show a statistical difference until the third measurement; Tables I and II). For example, in embedded specimens, Ca increased 7.2% by the second measurement ($p < 0.05$) and 13.4% by the fifth measurement ($p < 0.05$). Phosphorous showed similar variations in point mode, but the increases were less, for example, in embedded specimens P increased 9.6% ($p < 0.05$) by the fifth measurement.

In contrast to point mode, scan mode data for unembedded and embedded specimens showed small (not statistically significant) differences in the relative proportions of Ca, P, and C between the first measurement and the second, third, fourth, and fifth measurements (Tables I and II).

In both embedded and unembedded specimens at 200×, the apparent increases in Ca and P are associated with significant decreases in C. For example, in embedded specimens at 200×, C decreased 3.2% ($p < 0.05$) in point mode by the second measurement and decreased ~0.8% (not statistically significant) in scan mode by the fifth measurement (Table II).

In contrast to embedded specimens in scan mode at 200× that showed no statistical difference between any of the measurements, 1000× scan mode data showed

TABLE I Energy-dispersive x-ray data for PMMA-embedded specimens at 200×: Temporal variations in point mode (P) and scan mode (S) (mean values—mean ± standard deviation)

Spectra number	Wt % Ca	% Difference in Wt % Ca	WT % P	% Difference in Wt % P	Wt % C	% Difference in Wt % C
1P	21.90 ± 1.9[a]	—	9.83 ± 0.8[b]	—	67.59 ± 2.7[a]	—
2P	23.49 ± 2.1	7.23 ± 2.5	10.37 ± 1.1	5.44 ± 3.9	65.45 ± 3.1	–3.20 ± 1.3
3P	24.22 ± 2.1	10.66 ± 4.3	10.63 ± 1.0	8.28 ± 7.5	64.45 ± 3.2	–4.66 ± 2.4
4P	24.56 ± 2.1	12.23 ± 4.8	10.67 ± 1.0	8.69 ± 7.7	64.09 ± 3.1	–5.18 ± 2.5
5P	24.80 ± 2.1	13.35 ± 5.5	10.74 ± 0.9	9.62 ± 8.3	63.77 ± 3.0	–5.64 ± 2.7
1S	18.54 ± 0.8[c]	—	8.49 ± 0.4[c]	—	72.29 ± 1.3[c]	—
2S	18.74 ± 0.9	1.03 ± 0.9	8.53 ± 0.4	0.42 ± 0.9	72.09 ± 1.4	–0.28 ± 0.4
3S	18.82 ± 0.9	1.51 ± 0.8	8.56 ± 0.4	0.77 ± 1.1	71.93 ± 1.3	–0.49 ± 0.4
4S	18.90 ± 1.0	1.87 ± 0.9	8.62 ± 0.5	1.42 ± 1.3	71.80 ± 1.4	–0.67 ± 0.4
5S	18.97 ± 0.9	2.27 ± 1.2	8.63 ± 0.5	1.57 ± 1.6	71.73 ± 1.5	–0.78 ± 0.6

[a]Statistically significant differences existed between this measurement and the remaining measurements ($p < 0.05$), demonstrating the majority of the damage occurs with the initial measurements.
[b]Statistically significant differences existed between this measurements and measurements 3, 4, and 5 ($p < 0.05$).
[c]No statistical significant difference between the first measurement and any of the subsequent measurements (2, 3, 4, and 5).
Abbreviations: Ca = calcium, P = phosphorous, C = carbon.

TABLE II Energy-dispersive x-ray data for unembedded specimens at 200×: Temporal variations in point mode (P) and scan mode (S) (mean values—mean ± standard deviation)

Spectra number	Wt % Ca	% Difference in Wt % Ca	WT % P	% Difference in Wt % P	WT % C	% Difference in Wt % C
1P	23.06 ± 1.0[a]	—	10.42 ± 0.6[a]	—	65.85 ± 1.8[a]	—
2P	24.98 ± 1.6	8.29 ± 2.4	11.16 ± 0.7	7.06 ± 2.5	63.13 ± 2.4	–4.14 ± 1.4
3P	25.64 ± 1.7	11.16 ± 3.0	11.40 ± 0.8	9.40 ± 3.4	62.17 ± 2.6	–5.61 ± 1.8
4P	25.80 ± 1.8	11.81 ± 3.1	11.43 ± 0.9	9.61 ± 3.4	62.02 ± 2.8	–5.83 ± 1.9
5P	25.98 ± 2.0	12.59 ± 4.2	11.46 ± 0.9	9.88 ± 4.3	61.79 ± 3.0	–6.19 ± 2.3
1S	20.04 ± 0.8[b]	—	9.06 ± 0.4[b]	—	70.24 ± 1.2[b]	—
2S	20.16 ± 0.7	0.59 ± 1.7	9.16 ± 0.3	1.23 ± 1.8	70.04 ± 1.1	–0.33 ± 0.8
3S	20.25 ± 0.8	1.01 ± 1.2	9.13 ± 0.3	0.80 ± 1.4	70.03 ± 1.2	–0.35 ± 0.5
4S	20.41 ± 0.8	1.86 ± 2.2	9.20 ± 0.3	1.77 ± 2.3	69.74 ± 1.1	–0.75 ± 1.0
5S	20.33 ± 0.7	1.49 ± 2.0	9.19 ± 0.3	1.54 ± 2.7	69.83 ± 0.9	–0.62 ± 0.9

[a]Statistically significant differences existed between this measurement and the remaining measurements ($p < 0.05$), demonstrating the majority of the damage occurs with the initial measurements.
[b]No statistical significant difference between the first measurement and any of the subsequent measurements (2, 3, 4, and 5).
Abbreviations as in Table I.

TABLE III Energy-dispersive x-ray Data for PMMA-embedded specimens at 1000×: Temporal variations in point mode (P) and scan mode (S) (mean values—mean ± standard deviation)

Image number	Wt % Ca	% Difference in Wt % Ca	Wt % P	% Difference in Wt % P	Wt % C	% Difference in Wt % C
1P	23.35 ± 0.6[a]	—	10.07 ± 0.2[b]	—	65.91 ± 0.6[a]	—
2P	25.45 ± 0.5	9.01 ± 2.2	10.68 ± 0.8	6.02 ± 5.4	63.26 ± 1.2	–4.02 ± 1.5
3P	26.46 ± 0.5	13.33 ± 2.1	11.27 ± 0.6	11.89 ± 3.9	61.54 ± 1.2	–6.64 ± 1.5
4P	27.21 ± 0.6	16.53 ± 0.8	11.64 ± 0.2	15.69 ± 4.0	60.31 ± 0.8	–8.51 ± 0.7
5P	27.65 ± 0.8	18.31 ± 1.4	11.79 ± 0.1	17.13 ± 4.0	59.76 ± 0.4	–9.34 ± 0.8
1S	21.37 ± 0.1[a]	—	9.69 ± 0.1[b]	—	68.16 ± 0.2[b]	—
2S	21.70 ± 0.2	1.54 ± 1.0	9.82 ± 0.1	1.34 ± 0.7	67.80 ± 0.4	–0.52 ± 0.4
3S	21.95 ± 0.2	2.71 ± 0.4	9.95 ± 0.1	2.76 ± 1.2	67.36 ± 0.2	–1.17 ± 0.2
4S	22.16 ± 0.2	3.69 ± 0.6	9.96 ± 0.1	2.64 ± 0.7	67.24 ± 0.4	–1.35 ± 0.3
5S	22.44 ± 0.2	5.00 ± 0.4	10.12 ± 0.1	4.49 ± 1.6	66.74 ± 0.1	–2.07 ± 0.1

The changes noted in the mineral content at higher magnifications suggests that the majority of the damage is done within the first few interactions between the bone tissue specimen and the electron beam, resulting in alterations of the apparent mineral content.
[a]Statistically significant differences existed between this measurement and the remaining measurements ($p < 0.05$), demonstrating the majority of the damage occurs with the initial measurements.
[b]Statistically significant differences existed between this measurement and measurements 3, 4, and 5 ($p < 0.05$).
Abbreviations as in Table I.

significant changes in Ca by the second measurement, and by the third measurement significant changes were found in P and C (Table III). However, in contrast to scan mode data at 1000×, point mode data at 1000× showed trends similar to 200× embedded point mode data, with significant differences occurring by the second measurement for Ca, and C; and by the third measurement for P. However, point mode data at 1000× showed more dramatic increases in Ca by the second measurement than at 200× (9.0% vs. 7.2%, $p < 0.05$) and by the third measurement for P (11.9% vs. 8.3%, $p < 0.05$). In turn, C decreased slightly more (4.0%, $p < 0.05$) by the second measurement in point mode at 1000× than at 200× (3.2%, $p < 0.05$) (Table III).

Mineral Content Backscattered Electron Image Analysis

At 200×, BSE image gray level values increased (suggesting increased mineral content) by the second measurement in both scan and point mode (Fig. 2). This occurred in both embedded and unembedded specimens. Results in Tables I and II show that these artifactual changes in apparent mineral content are associated with "burning-off" of carbon and other light elements.

Compared with 200×, results at 1000× (all specimens were embedded in this analysis) showed even larger changes in apparent mineral content by the second measurement in scan mode (1.2% vs. 3.6%) and the final (second) measurement in point mode (5.9% vs. 18.6%, $p < 0.05$) (Fig. 2).

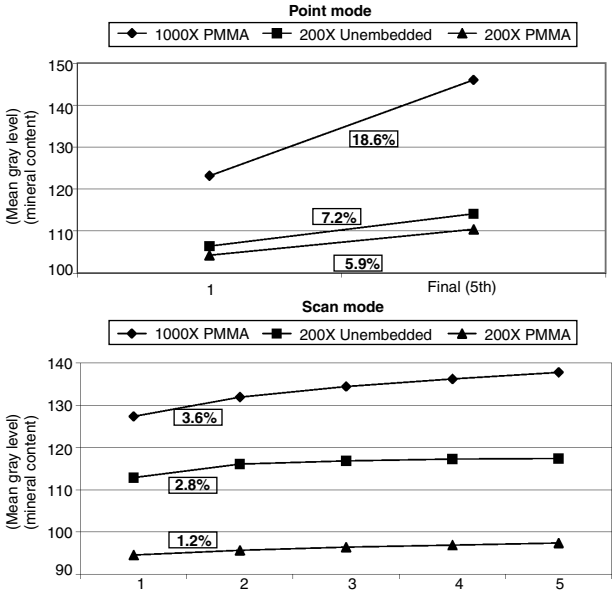

FIG. 2 Backscattered electron image mean gray level variations (mineral content): Scan and point mode data (percentages in boxes indicate differences between first two data points).

Figure 1 demonstrates deleterious effects of multiple analyses in point mode on BSE image gray levels. The "bleaching" of the analyzed region demonstrates an artificial increase in mineral content due to electron beam-induced damage.

Discussion

Tissue damage caused by the electron beam is one of the most important confounding factors in quantitative BSE image analysis of bone mineral content. Results of our coupled BSE/EDX analyses at sequential time intervals allowed for the assessment of temporal variations in this observable damage. In conventional BSE/EDX analyses of bone, this damage is typically recognized as changes in proportions of elements in microprobe analyses and/or artifactual "bleaching" in BSE images. The results of point mode and/or high magnification scanning conditions examined in this study support the first hypothesis that conventional imaging conditions can produce significant damage during the first measurement. However, the impact of this damage on relative proportions of C, Ca, and P, and on apparent mineral content was minimal (<1.5%) within the first measurement in the embedded specimens analyzed in scan mode at 200×. In contrast, point mode data in embedded specimens suggest that the change within the first measurement can be on the order of 7%. In general, these results suggest that mineral content measurements can be reliable when using coupled BSE/EDX analyses of PMMA-embedded bone if lower magnifications are used in scan mode, and if prolonged exposure to the electron beam is avoided. This conclusion reaffirms the use of what can be considered conventional methods in quantitative BSE image analysis of bone mineral content—PMMA embedding, scan mode, and the use of nominal magnifications typically on the order of ~200× (Bloebaum *et al*. 1997, Boyde *et al*. 1995, Kingsmill and Boyde 1998, Skedros *et al*. 1993a, Vajda and Skedros 1999, Vajda *et al*. 1998).

The second hypothesis, that point mode is relatively more deleterious than scan mode, was supported by EDX data in embedded and unembedded specimens—damage in point mode was obvious by the second or third measurements at 200× and 1000×. In addition, our extrapolations show that in some situations (e.g., 1000×, point mode) mineral content can be significantly affected within the first measurement. Extrapolation using the first and second EDX measurements in point mode also suggests that significant damage occurs during the first measurement regardless of whether or not the bone tissue was embedded in PMMA (Fig. 3). In contrast, changes that occur within the first EDX measurement in scan mode at 200× are minor. Extrapolation of BSE image gray level data at 200× and 1000× also suggests that the damage within the first measurement produced minor (~3-4%) changes in mean gray level in scan mode when compared with point mode (~6-23%) (Fig. 4). Empirical data suggest that these "minor" changes in mean gray levels are negligible in the context of actual mineral content variations (Bloebaum *et al*. 1997; Skedros *et al*. 1993a,b). In other words, these quantitative

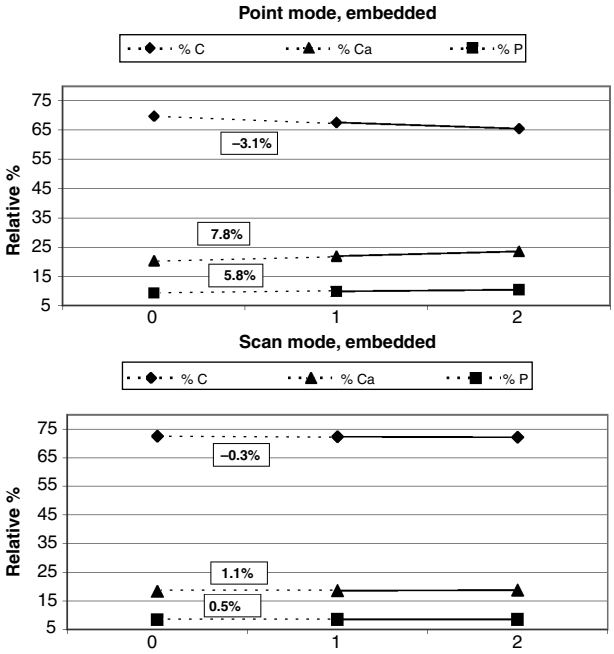

FIG. 3 Linear extrapolation (—), energy-dispersive x-ray data (200×). Note that greater relative % change occurs in point mode versus scan mode, indicating that point mode is more deleterious than scan mode. The extrapolations in this graph also show that in point mode significant damage occurs regardless of whether or not the bone was embeded in PMMA.
Abbreviations as in Table I.

atomic number-contrast analysis methods are not sufficiently sensitive for detecting mineral content differences of this order of magnitude. This lack of sensitivity, which can be attributed to surface topography and inherent circuit "noise" (Vajda *et al*. 1998), is not universally recognized as an important confounding variable when interpreting mineral content variations in BSE images of bone (Loveridge *et al*. 2004, Roschger *et al*. 1998, Vajda and Skedros 1999).

In contrast to analyses in scan mode, analyses in point mode included focusing the electron beam on a smaller area, which increased the energy dose absorbed by the specimen. In the context of differences in the extent of damage induced by scan versus point mode, it is important to mention here that the incident electron dose that impinges on the specimen is often not the same as the electron dose absorbed by the specimen (Goldstein *et al*. 1992 pgs. 662–668). An additional distinction between scan and point mode is the amount of x-ray photons collected from the relatively larger collection area; in scan mode this may be decreased proportionally because the energy absorbed by the analyzed region was also relatively reduced. This helps explain the relatively smaller increases in Ca and P, and smaller decreases in C in scan mode when compared with point mode. Compared with scan mode, the relative size of the electron interaction volume in point mode is also increased with respect to the imaged area at the specimen surface. In turn, it would be suspected that this produces greater damage, which is obvious when a BSE image is taken of a region where serial point-mode measurements have been made (Fig. 1).

The third hypothesis was supported by data in embedded specimens showing that deleterious effects were greater at 1000× than at 200×. This finding is important since the analysis of minute regions within bone microstructure, such as cement lines and interlamellar seams, require high magnification and small analysis regions. Holmes *et al*. (2000) also suggested that probe currents below 2.0 nA help reduce "bleaching" artifact when point mode is required at high magnification. Based on this suggestion, Skedros *et al*. (2005) rendered the "bleaching" artifact negligible in a study of cement line mineral content in 1500× images by using point mode with a probe current of 0.75 nA. These observations reinforce the importance of considering the influences of magnification, point versus scan mode, and probe current on damage-induced artifact in quantitative BSE/EDX analyses of bone mineral content.

Point mode data at 200× reject the fourth hypothesis that consequences of the observable damage in PMMA-embedded tissues are less significant than the damage that occurs in unembedded bone (Tables I and II). Embedded and unembedded tissues showed no significant changes in the relative percent of Ca, P, or C in scan mode. Furthermore, in nearly all cases (only %P differs slightly), point mode data at 200× for embedded and unembedded specimens showed similar percent differences and significant differences between the first measurement and the remaining measurements.

Supporting the fifth hypothesis, the data showed that the apparent increases in Ca and P likely result from significant decreases in C and other relatively light elements: –3.2% ($p < 0.05$) in point mode by the second measurement and –0.8% (not statistically significant) in scan mode by the fifth measurement in embedded specimens. Previous investigations have shown that low atomic number elements are more easily lost than high atomic number elements during BSE imaging of polymer embedding materials and bone (Boyde and Jones 1996, Thach and Thach 1971, von Zglinicki 1993). One limitation of the present study was that the actual mineral content of the bone was not known prior to analysis. Consequently, it was not possible to determine exactly the degree of damage incurred during the first measurement. However, the extrapolations described above and illustrated in Figures 3 and 4 support the possibility that in some cases this damage can be significant relatively early in a microanalysis session. However, the minor alterations in apparent mineral content shown in some scanning conditions support results of previous studies using various standards, artificial bone, and/or ashed bone specimens that mineral content can be reliably determined using EDX spectroscopy and/or quantitative BSE imaging techniques (Boyde *et al*. 1995, Loveridge *et al*. 2004, Roschger *et al*. 1998, Vajda *et al*. 1998). Another limitation involves our inability to measure energy absorbed by the specimen. These data would help express our findings more clearly, especially since there are myriad additional variables involved in the damage process, including topographic changes of the altered surface, and surface

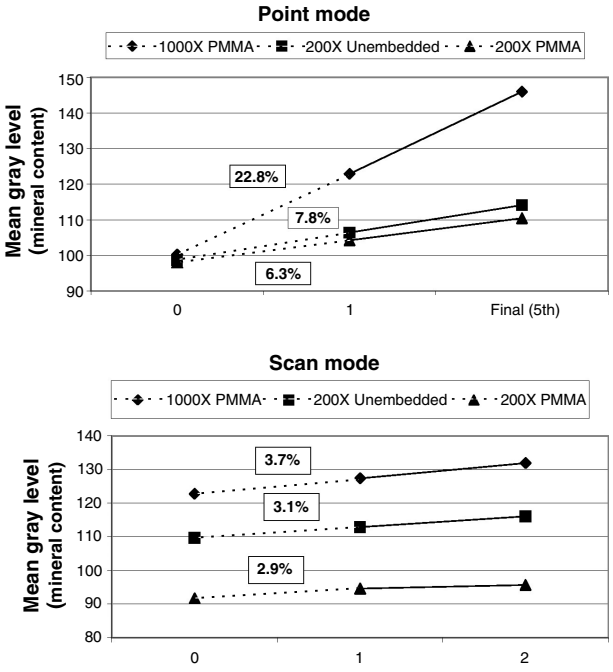

FIG. 4 Linear extrapolation (—), backscattered electron image mean gray level data. The relatively minor mineral content changes that occur in scan mode versus point mode support the second hypothesis that point mode is relatively more deleterious than scan mode.

charging (Vajda and Skedros 1999, Vajda *et al*. 1998). The use of gold (Z = 79) as a conductive surface coating is also being supplanted by carbon (Z = 6) when using BSE imaging for quantitative mineral content analyses of bone. This is because carbon has less influence on mean atomic number contrast since it is more similar to bone (Z ~ 10–12) (Skedros *et al*. 1993b). However, empirical studies have demonstrated that very thin gold coatings do not diminish the resolution of subtle variations in relative mineral content in microscopic or macroscopic regions of bone (Skedros *et al*. 2005, Vajda and Skedros 1999, and unpublished data). Nevertheless, comparative studies are needed for better understanding of the strengths and limitations of gold versus carbon coatings in quantitative and mineral content analyses, including investigating the probability that they have different influences in the development and magnitude of electron beam damage.

Conclusions

Results of this quantitative study clearly demonstrate that apparent mineral content can be artifactually altered during BSE/EDX analyses under conventional scanning conditions. This alteration was associated with the loss of C and other low atomic number elements. However, negligible effects were found when low magnification and short analysis times were used. At 200×, the consequences of damage were similar in embedded and nonembedded specimens. When using magnification on the order of 1000× it was clear that artifactual mineral content changes associated with increased magnification, embedding, and scan/point mode can be substantially greater. In conclusion, quantitative mineral content analysis in BSE images can be reliable in embedded tissue if magnification and accelerating probe current are as low as possible (especially when using point mode) and analysis is limited to only one x-ray spectrum or BSE image in a given region.

Acknowledgments

The authors thank Scott M. Sorenson for his assistance in completing this manuscript. The authors also wish to acknowledge the Office of Research and Development (R&D), Medical Research Service, Department of Veterans Affairs (VA) Salt Lake City Health Care System and the Department of Orthopedics, University of Utah School of Medicine.

References

Acosta DR, Vazquez-Polo G, Garcia R, Castano VM: Electron beam degradation of Ca-A zeolite. *Radiat Effects Defects Sol* 127, 37–43 (1993)

Bloebaum RD, Bachus KN, Boyce TM: Backscattered electron imaging: The role in calcified tissue and implant analysis. *J Biomater Appl* 5, 56–85 (1990)

Bloebaum RD, Skedros JG, Vajda EG, Bachus KN, Constantz BR: Determining mineral content variations in bone using backscattered electron imaging. *Bone* 20, 485–490 (1997)

Boyce TM, Bloebaum RD, Bachus KN and Skedros JG: Reproducible methods for calibrating the backscattered electron signal for quantitative assessment of mineral content in bone. *Scanning Microsc* 4, 591–600, discussion 600–603 (1990)

Boyde A, Jones SJ: Scanning electron microscopy of bone: instrument, specimen, and issues. *Microsc Res Tech* 33, 92–120 (1996)

Boyde A, Compston JE, Reeve J, Bell KL, Noble BS, Jones SJ, Loveridge N: Effect of estrogen suppression on the mineralization density of iliac crest biopsies in young women as assessed by backscattered electron imaging. *Bone* 22, 241–250 (1998)

Boyde A, Jones SJ, Aerssens J, Dequeker J: Mineral density quantitation of the human cortical iliac crest by backscattered electron image analysis: Variations with age, sex, and degree of osteoarthritis. *Bone* 16, 619–627 (1995)

Everhart TE, Herzog RF, Chang MS, DeVore WJ: Electron energy dissipation measurements in solids. In *Proceedings of the 6th International Conference on X-Ray Optics and Microanalysis* (Eds. Shinoda G, Kohra K, Ichinokawa T). Tokyo, Japan, (1972) 81–86

Fryer JR, McConnell CH: Effect of temperature on radiation damage to aromatic organic molecules. *Ultramicroscopy* 40, 163–169 (1992)

Goldstein JI, Newbury DE, Echlin P, Joy DC, Romig AD, Lyman CE, Fiori C, Lifshin E: *Scanning Electron Microscopy and X-Ray Analysis: A Text for Biologists, Materials Scientist, and Geologists*. Plenum Press, New York (1992) 820

Holmes JL, Bachus KN, Bloebaum RD: Thermal effects of the electron beam and implications of surface damage in the analysis of bone tissue. *Scanning* 22, 243–248 (2000)

Isaacson M: Specimen damage in the electron microscope. *Principles and Techniques of Electron Microscopy*. Van Nostrand Reinhold Company, New York, (1977) 1–78

Kingsmill VJ, Boyde A: Mineralisation density of human mandibular bone: Quantitative backscattered electron image analysis. *J Anat* 192 (Pt. 2), 245–256 (1998)

Kuo TY, Skedros JG, Bloebaum RD: Comparison of human, primate, and canine femora: Implications for biomaterials testing in total hip replacement. *J Biomed Mater Res* 40, 3, 475–489 (1998)

Loveridge N, Power J, Reeve J, Boyde A: Bone mineralization density and femoral neck fragility. *Bone* 35, 929–941 (2004)

Misof BM, Roschger P, Cosman F, Kurland ES, Tesch W, Messmer P, Dempster DW, Nieves J, Shane E, Fratzl P, Klaushofer K, Bilezikian J, Lindsay R: Effects of intermittent parathyroid hormone administration on bone mineralization density in iliac crest biopsies from patients with osteoporosis: a paired study before and after treatment. *J Clin Endocrinol Metab* 88, 1150–1156 (2003)

Nicholson WA, Dempster DW: Aspects of microprobe analysis of mineralized tissues. *Scan Electron Microsc* 517–533 (1980)

Roschger P, Plenk H, Jr., Klaushofer K, Eschberger J: A new scanning electron microscopy approach to the quantification of bone mineral distribution: Backscattered electron image grey-levels correlated to calcium Kα-line intensities. *Scan Microsc* 9, 75–88 (1995)

Roschger P, Fratzl P, Klaushofer K, Rodan G: Mineralization of cancellous bone after alendronate and sodium fluoride treatment: a quantitative backscattered electron imaging study on minipig ribs. *Bone* 20, 393–397 (1997)

Roschger P, Fratzl P, Eschberger J, Klaushofer K: Validation of quantitative backscattered electron imaging for the measurement of mineral density distribution in human bone biopsies. *Bone* 23, 319–326 (1998)

Ruff CB and Hayes WC: Cross-sectional geometry of Pecos Pueblo femora and tibiae–A biomechanical investigation: I. Method and general patterns of variation. *Am J Phys Anthrop* 60, 359–381 (1983)

Sanderson C, Kitabayashi LR: Parallel experience of two different laboratories with the initiator perkadox 16 for polymerization of methylmethacrylates. *J Histotechnol* 17, 343–348 (1994)

Skedros JG, Bloebaum RD, Bachus KN, Boyce TM: The meaning of graylevels in backscattered electron images of bone. *J Biomed Mater Res* 27, 47–56 (1993a)

Skedros JG, Bloebaum RD, Bachus KN, Boyce TM, Constantz B: Influence of mineral content and composition of graylevels in backscattered electron images of bone. *J Biomed Mater Res* 27, 57–64 (1993b)

Skedros JG, Holmes JL, Vajda EG, Bloebaum RD: Cement lines of secondary osteons in human bone are not mineral deficient: New data in a historical perspective. *Anatom Rec* (in press) (2005)

Thach RE, Thach SS: Damage to biological samples caused by the electron beam during electron microscopy. *Biophys J* 11, 204–210 (1971)

Vajda EG, Skedros JG: Primary difficulties in quantitative backscattered electron (BSE) imaging. *Bone* 24, 619–621 (1999)

Vajda EG, Bloebaum RD and Skedros JG: Validation of energy dispersive x-ray spectrometry as a method to standardized backscattered electron images of bone. *Cells Mater* 6, 79–92 (1996)

Vajda EG, Skedros JG, Bloebaum RD: Errors in quantitative backscattered electron analysis of bone standardized by energy-dispersive x-ray spectrometry. *Scanning* 20, 527–535 (1998)

Vajda EG, Humphrey S, Skedros JG, Bloebaum RD: Influence of topography and specimen preparation on backscattered electron images of bone. *Scanning* 21, 379–387 (1999)

von Zglinicki T: Radiation damage and low temperature x-ray microanalysis. In *X-Ray Microanalysis in Biology: Experimental Techniques and Applications*. Cambridge University Press, Cambridge, (1993) 117–132

Weavers BA: The analytical electron microscope, EMMA-4. In *Principles and Techniques of Electron Microscopy*. Van Nostrand Reinhold Company, New York, (1975) 174–244